

Article

Experimental Study of the Temperature Distribution in CRTS-II Ballastless Tracks on a High-Speed Railway Bridge

Lei Zhao , Ling-Yu Zhou, Guang-Chao Zhang , Tian-Yu Wei, Akim D. Mahunon, Li-Qiang Jiang * and Ying-Ying Zhang

School of Civil Engineering & National Engineering Laboratory for High Speed Railway Construction, Central South University, 68 South Shaoshan Road, Changsha 410075, China; zl402207991@csu.edu.cn (L.Z.); zhoulingyu@csu.edu.cn (L.-Y.Z.); zhang24@csu.edu.cn (G.-C.Z.); 174812275@csu.edu.cn (T.-Y.W.); mahunonakim@csu.edu.cn (A.D.M.); z184812279@csu.edu.cn (Y.-Y.Z.)

* Correspondence: jianglq2019@csu.edu.cn

Received: 8 January 2020; Accepted: 6 March 2020; Published: 13 March 2020



Abstract: To study the temperature distribution in the China Railway Track System Type II ballastless slab track on a high-speed railway (HSR) bridge, a 1:4 scaled specimen of a simply-supported concrete box girder bridge with a ballastless track was constructed in laboratory. Through a rapid, extreme high temperature test in winter and a conventional high temperature test in summer, the temperature distribution laws in the track on the HSR bridge were studied, and the vertical and transverse temperature distribution trend was suggested for the track. Firstly, the extreme high temperature test results showed that the vertical temperature and the vertical temperature difference distribution in the track on HSR bridge were all nonlinear with three stages. Secondly, the extreme high temperature test showed that the transverse temperature distribution in the track was of quadratic parabolic nonlinear form, and the transverse temperature gradient in the bottom base was significantly higher than that of the other layers of the track. Thirdly, the three-dimensional temperature distribution in the track on HSR bridge was a nonlinear, three-stage surface. Furthermore, similar regularities were also obtained in the conventional high temperature test, in which the temperature span ranges were different from those of the extreme high temperature test. In addition, the conventional high temperature test also showed that under the natural environment conditions, the internal temperature gradient in the track layers changed periodically (over a period of 24 h).

Keywords: high-speed railway bridges; China railways track system; ballastless track; concrete box girder; temperature distribution

1. Introduction

The China Railway Track System Type II (CRTS-II) ballastless slab track is widely used in China's national high-speed railway system, due to its various advantages, such as running comfort and high structural stability [1–3]. As the ballastless track–bridge structural system composed of CRTS-II slab track is a vertical multilayer spatial structure, the local temperature and overall temperature are significant factors that inevitably impact the mechanical properties of the structural system and affect the running comfort and safety of the high-speed trains, increasing the difficulty of maintenance. Thus, the influence of the temperature on the mechanical performance of the track structure cannot be ignored [4,5].

Recently, scholars have carried out theoretical and experimental studies on the temperature distribution of bridge structures [6–10]; analyzed a series of influencing factors on the temperature

and stress distributions in concrete box girder bridges; and presented analytical models to predict temperature and stress distributions. The temperature distributions in concrete box-girder bridges were analyzed [11–15] and empirical formulas were proposed to predict the maximum vertical and lateral temperature gradients. As one of the most significant factors producing interfacial cracks [16] and longitudinal buckling [17] in ballastless tracks, the temperature distribution has a great influence on the thermal behavior of ballastless tracks [18–22]. The main causes of the structural diseases in ballastless track structures are the variation of the ambient temperature and the difference in thermal behavior between the cement emulsified asphalt mortar (the CA mortar) and the concrete [23–25]. In recent years, research on the temperature distribution in CRTS-II ballastless tracks has increased. However, most existing research has focused on track slabs with subgrades [26–28]. The few studies on the temperature distribution in CRTS-II ballastless tracks on high-speed railway (HSR) bridges mainly focused on the theoretical solution under periodic climate conditions [29]. In addition, the existing research methods on temperature distribution analysis mainly included theoretical analysis methods based on finite element calculations and statistical analysis methods based on monitoring tests. Yan et al. [30] established a thermodynamic analysis model of CRTS-II ballastless track based on finite element software and studied the vertical temperature distribution of the ballastless tracks under different climatic conditions, but due to the lack of accurate thermodynamic parameters of the CA mortar in the model, it was difficult to form a comprehensive understanding of the overall temperature distribution in the track. Dai et al. [29] fitted the average vertical temperature difference distribution in the track by exponential function and obtained the daily changing law of the transverse temperature distribution in the ultra-high section of the track based on statistical analysis of the daily temperature data monitored on a CRTS-II ballastless track. However, due to the lack of temperature gauges in the CA mortar, the transverse and vertical temperature distribution in the track cannot be completely described. In summary, there is still no heating test method to control the temperature rise and drop in ballastless tracks. Little attention has been paid to the CA mortar layer, and research on the transverse and vertical temperature distribution under rapid, extreme high temperature rising and dropping conditions is scarce. Meanwhile, due to global warming, the extreme high temperatures are becoming more frequent, and rapid temperature rising and dropping is inevitable.

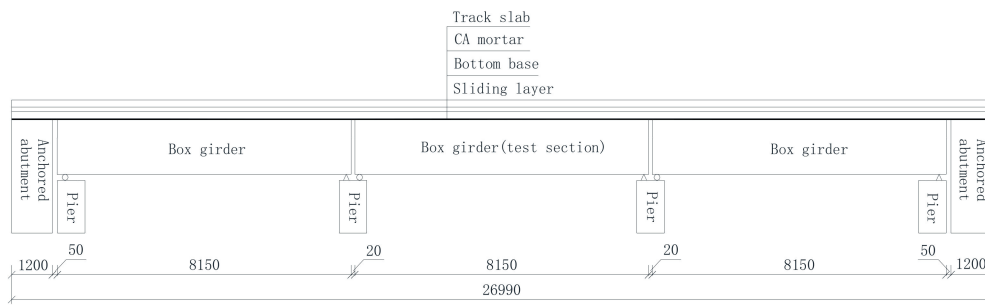
In addition, although the existing research produced some satisfactory conclusions on the temperature distribution in the CRTS-II ballastless track-bridge system under high-temperature conditions [29], the research considered only the direct solar irradiation in natural climates, and the results presented a non-uniform temperature distribution. Based on finite element model, Zhu et al. [31] concluded that the shadowing effect has a great influence on the temperature distribution in the box girder of ballastless tracks. However, there is currently a lack of research on the uniform temperature distribution of CRTS-II ballastless tracks on HSR bridges under sunlight occlusion or cloudy weather conditions. Moreover, no specification of the temperature profile of CRTS-II ballastless tracks on HSR bridges exists in the codes.

In this paper, a 1:4 scaled specimen of simply supported concrete box girder bridge with ballastless track was constructed. The rapid extreme high temperature (EHT) test was carried out in winter in the national engineering laboratory of high-speed railway construction technology of Central South University. In summer of the same year, a typical high temperature day was selected, and conventional high temperature (CHT) test was carried out on the scaled specimen under no direct sunlight conditions. The results were analyzed and compared with the relevant literature to obtain meaningful conclusions. Using the temperature sensor system, the transverse and vertical temperature distributions in the track on a HSR bridge under different temperature conditions were studied, and the conclusions can provide references for the design of CRTS-II ballastless tracks and further understanding of the effect of temperature on CRTS-II ballastless tracks on HSR bridges.

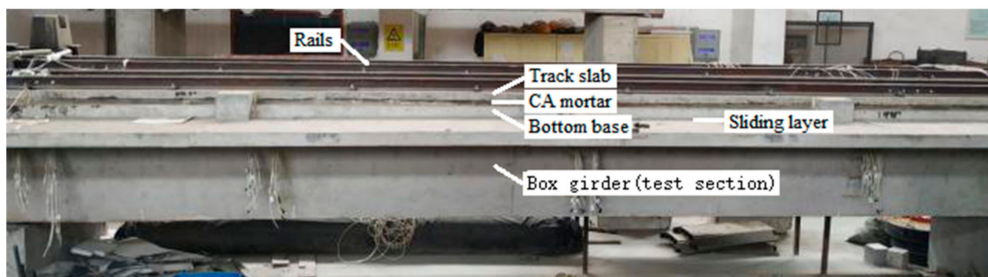
2. Experimental Program

2.1. Design and Construction of the Specimen

The HSR bridge with a CRTS-II ballastless track is composed of simply supported box girder and CRTS-II ballastless track. The prototype girder is a 31.5 m standard post-tensioned precast, prestressed simply supported concrete box girder. The track is composed of the rail, elastic fasteners, track slab, CA mortar layer, bottom base, geotextile sliding layer, high strength extrusion plate, lateral block and anchor structure behind the platform. Based on the principle of geometry similarity, the 1:4 scaled specimen was constructed, and its facade design drawing is shown in Figure 1.



(a) Facade design drawing of the specimen (unit: mm)



(b) Scaled specimen diagram (test section)

Figure 1. The scaled specimen of the high-speed railway (HSR) bridge with ballastless tracks.

The scaled specimen constructed in this paper was mainly based on the equivalence principle, as follows: Firstly, the shape of the scaled specimen was consistent with that of the prototype, meeting the geometric similarity conditions (the geometric similarity ratio in this paper was 1:4). Secondly, the stress similarity ratio was 1, meaning the upper and lower concrete edges stress of the scaled specimen were equal to those of the prototype under the action of train load. Thirdly, the materials used in the construction of the specimen were all consistent with those of the prototype. Fourthly, the boundary conditions of the scaled specimen were identical to those of the prototype structure.

To ensure the continuity of the track with the HSR bridge and the consistency of the stress state, two simply supported concrete box girders with the same size and structural form were designed at both ends of the test specimen, forming a three-span ballastless track-bridge structural system, and the track was continuously arranged throughout the bridge. In addition, to accurately simulate the constraints of the infinite length of the track system, the bridge abutment was made with solid concrete blocks with anchored steel bars embedded in the abutment and the bottom base. Meanwhile, the abutment and the foundation were also anchored. The cross-section size of the specimen is shown in Figure 2b.

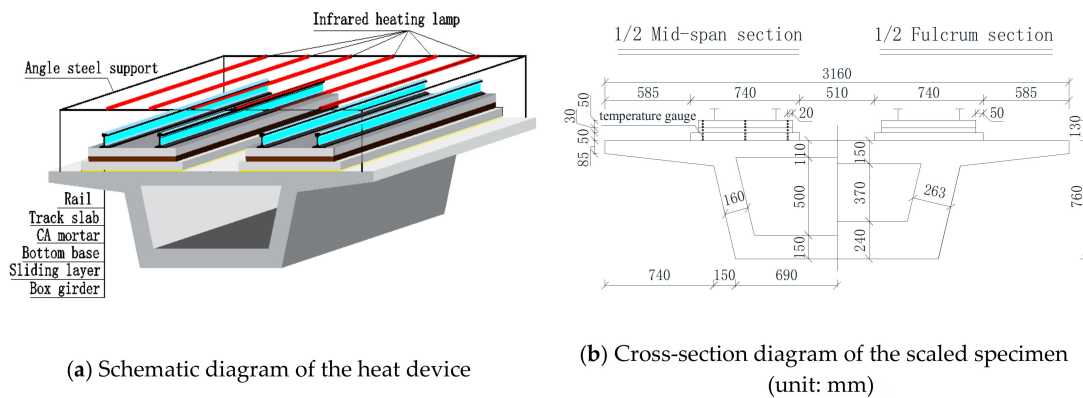


Figure 2. The extreme high temperature (EHT) test device diagram.

The materials used in the construction of the scaled specimen were all consistent with those of the prototype structure. The track slab and box girder were made of C50 grade concrete, and the bottom base was made of C30 grade concrete, and the measured strength and Young's modulus of the CA mortar satisfied the requirements.

2.2. Temperature Test Device

To accurately simulate the temperature rising and dropping on the track, a set of heat devices and a set of temperature control systems were designed. The heat device was mainly composed of angle steel supports and infrared heating lamps. The length of a single infrared heating lamp was 1.2 m with a rated power of 1.2 kW. Eight (8) identical angle steel supports were arranged along the longitudinal direction of the track. The longitudinal span and transverse length of each angle steel support was 1.2 m and 2.5 m, respectively; and the angle steel support was 0.2 m over the top surface of the track slab. Six (6) lamp tubes were uniformly arranged on each angle steel support, as shown in Figure 2a. To reduce the heat loss, the periphery of the heating device was covered with tinfoil paper and an aluminum silicate fiber blanket.

The temperature control system was mainly composed of temperature gauges and temperature controllers. The temperature gauges were arranged on the surface of the track slab under the heat device, and the temperature signal was passed onto the temperature controller. After setting the maximum heating temperature, the lamp tube could be turned off automatically when the temperature reached the maximum value set and the lamp tube would be turned on automatically when the temperature decreased 1 °C below that value to achieve the purpose of heating at constant temperature. The precision of the constant temperature control was ± 1 °C.

The JMT-36B semiconductor temperature gauges were embedded in the track. The 7 temperature gauges were distributed along the depth of the track in its middle and both sides of the cross-section, and there were seven layers along the vertical direction of the track, as shown in Figure 2b. The interlayer gauge data belonged to both the bottom surface temperature of the upper layer and the top surface temperature of the bottom layer. The data were collected by JMZX-3001 comprehensive tester (Kingmach Measurement&Monitoring Technology Co., Ltd, Changsha, China) with an accuracy of ± 0.1 °C.

2.3. Determination of the Maximum Temperature Value

Based on statistical analysis of atmospheric temperature over a 50-year time period, Lou et al. [32] concluded that the maximum extreme temperature of the ballastless track on HSR bridge could reach 57.77 °C. In addition, the Chinese railway design code TB-10002 [33] stipulated that the annual average maximum temperature difference between winter and summer was 50 °C. Combined with the above considerations, the temperature difference span of the EHT test was designed to be 50 °C. To allow the temperature difference to easily reach the designed maximum value, the experimental time was chosen to be winter season. The air temperature in the laboratory during the test was 8 °C; thus, the heating

started at 8 °C and increased to 58 °C. When the maximum temperature was reached, the temperature control system regulated the heating system automatically, and the temperature was maintained at 58 ± 1 °C for a period of time such that the temperature of the track could rise to a certain extent. After that, the heating system was turned off to simulate the natural temperature drop.

To compare the results of the EHT test with the results of the conventional high temperature test obtained under typical, no direct sunshine, high temperature conditions, the CHT test was performed in the summer of the same year. The Chinese railway design code TB-10002 [33] provided the annual national summer mean temperature in July based on the statistics of the Central Weather Bureau. The data show that the city of Changsha, located in the central south area of China, is one of the regions with the highest temperature during summer. Thus, the results of the CHT test in this area could be used as typical representative of the most critical temperature load in China. The date of the CHT test was selected to be a period when the weather was sunny, and the temperature of several consecutive days was kept around the annual maximum temperature of 38 °C. The condition of the CHT test required that the doors and windows were opened to provide good ventilation in the laboratory. The CHT test correctly simulated the uniform temperature distribution in the track under no direct sunshine conditions. The data of the CHT test were collected every 30 min, and the test was carried out from 9:00 to 9:00 of the next day.

3. Vertical Temperature Distribution

3.1. Temperature-Time Relationship

The EHT test was carried out in winter with an initial temperature of 8 °C. The whole EHT test process lasted 290 min with a temperature rising period of 185 min and a natural dropping period of 105 min, as shown in Figure 3a. The CHT test coincided with the high temperature weather conditions in summer; the weather was sunny on the test day and the whole process lasted 24 h. During the CHT test, the highest air temperature under solar irradiation (38.0 °C) occurred at 15:30, as shown in the temperature-time curves of Figure 3b.

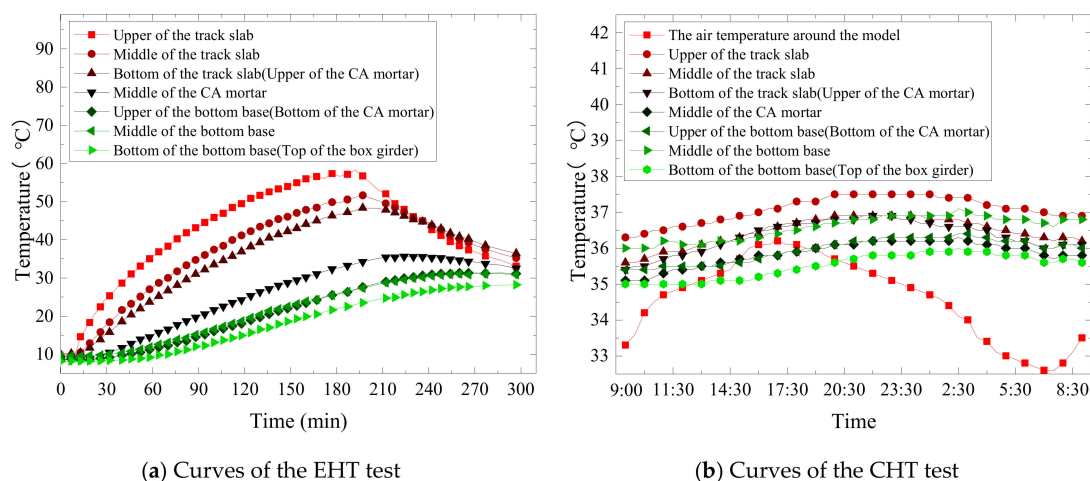


Figure 3. Vertical temperature-time curves.

In Figure 3a, the temperature-time curves of the EHT test show that the top surface of the track slab heated up quickly to reach a highest value of 58.2 °C with a temperature difference of 50.2 °C. In the temperature dropping period, the top surface temperature of the track slab decreased quickly to 33.1 °C at the end of the test. The vertical temperature-time curves of the track slab intersected, resulting in a negative temperature gradient (the temperature gradient is considered positive when the temperature of the upper layer is higher than that of the lower layer; otherwise it is considered negative). During the whole test process, the temperature-time curves of the track layers were similar.

The curve between the upper and the middle part of the CA mortar was obvious. The temperature difference in this layer was large, and there was an obvious difference in the temperature conduction of the layers. The greater the depth from the top surface of the track slab to the temperature measurement point, the more obvious the temperature conduction lag.

In Figure 3b, the temperature–time curves of the CHT test show that under no direct sunshine conditions in summer, the air temperature around the test specimen first increased and then decreased with a sinusoidal trend. The minimum temperature (32.6 °C) occurred at 07:00, and the maximum temperature (36.2 °C) occurred at 17:00. The temperature–time curves of the track layers were similar, but the temperature lagged behind the air temperature. The maximum temperature of the top surface of the track slab (37.5 °C) occurred in the time period from 20:00 to 01:00. The temperature in the track layers decreased gradually from the top to the bottom. Although the temperature of the middle part of the bottom base was slightly lower than that of the bottom surface and center of the track slab, it was still higher than that of the other layers, indicating that the thermal insulation effect in the bottom layer of the track is high.

3.2. Vertical Temperature Gradient

To study the most critical layer affected by temperature in both the EHT test and the CHT test, the temperature gradient in each layer and interlayer of the track was analyzed, and the results are shown in Figure 4.

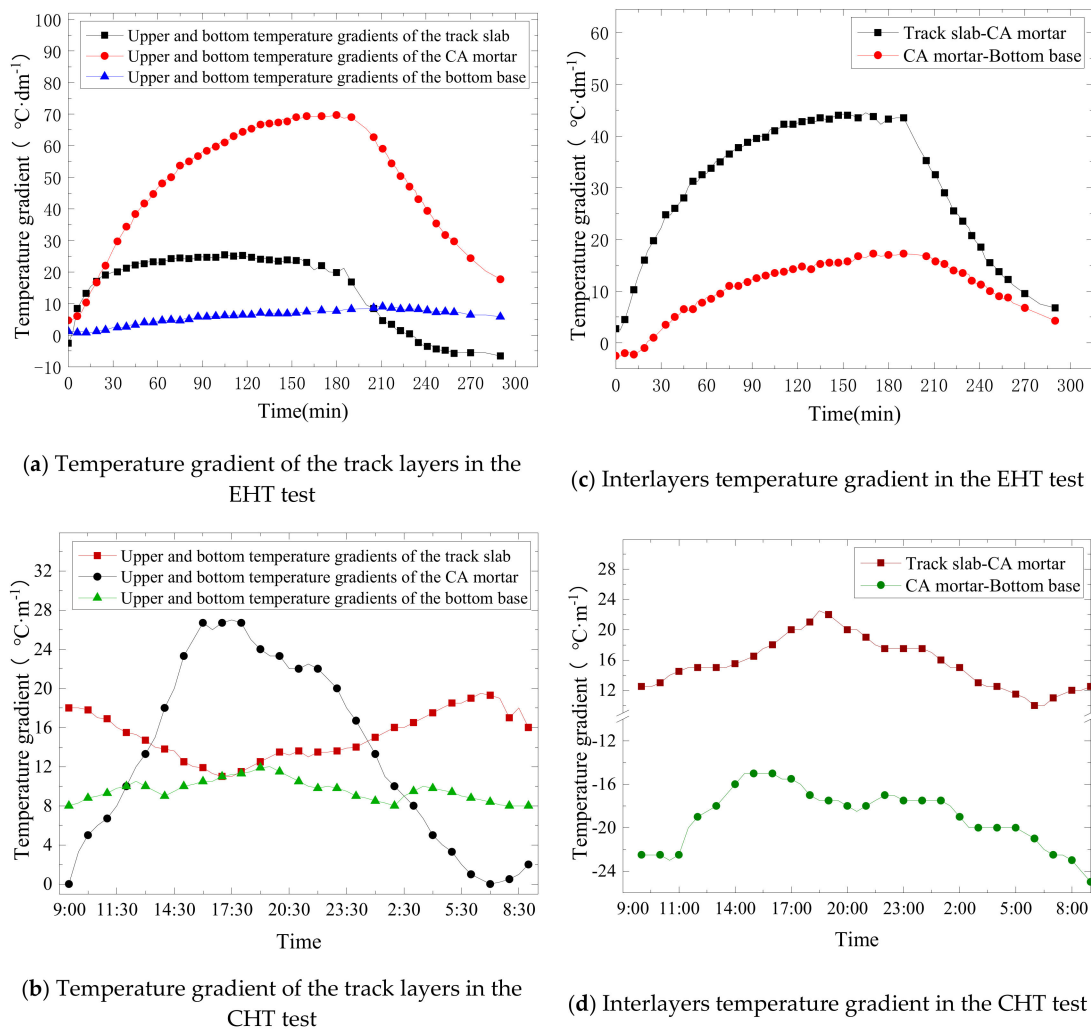


Figure 4. Vertical temperature gradient–time curves.

Figure 4a shows that the maximum vertical temperature gradient in the track slab was $25.4\text{ }^{\circ}\text{C}\cdot\text{dm}^{-1}$. A negative temperature gradient appeared in the layer when the temperature decreased, and the maximum negative temperature gradient was $-6.6\text{ }^{\circ}\text{C}\cdot\text{dm}^{-1}$. The vertical temperature gradient curves in the bottom base were even, with a small variation range, and the maximum vertical temperature gradient was only $8.0\text{ }^{\circ}\text{C}\cdot\text{dm}^{-1}$; thus, the bottom base was the less affected by the vertical temperature gradient in the track. The maximum vertical temperature gradient in the CA mortar layer was $69.7\text{ }^{\circ}\text{C}\cdot\text{dm}^{-1}$. Throughout the whole EHT test process, the vertical temperature gradient in the CA mortar layer was higher than that of the other layers; therefore, the CA mortar layer was the most critical layer under the action of temperature.

Figure 4b shows that the temperature gradients in the track layers were all positive and changed periodically with a period span of 24 h. The vertical temperature gradient in the track slab first decreased and then increased; a minimum value of $11.0\text{ }^{\circ}\text{C}\cdot\text{m}^{-1}$ occurred at 17:00, and a maximum value of $19.5\text{ }^{\circ}\text{C}\cdot\text{m}^{-1}$ occurred at 6:00. The vertical temperature gradient in the bottom base first increased and then decreased; a minimum value of $8.0\text{ }^{\circ}\text{C}\cdot\text{m}^{-1}$ occurred at 08:00, and a maximum value of $12.0\text{ }^{\circ}\text{C}\cdot\text{m}^{-1}$ occurred at 19:30. The vertical temperature gradient in the CA mortar layer first increased and then decreased; a minimum value of $0\text{ }^{\circ}\text{C}\cdot\text{m}^{-1}$ occurred at 07:00, and a maximum value of $27.0\text{ }^{\circ}\text{C}\cdot\text{m}^{-1}$ occurred at 17:30. The temperature gradient and its variation range were the largest in the CA mortar; therefore, the CA mortar layer was the most affected by the vertical temperature gradient.

Figure 4c shows that the maximum vertical temperature gradient between the CA mortar and the bottom base was $17.3\text{ }^{\circ}\text{C}\cdot\text{dm}^{-1}$ and that between the track slab and the CA mortar was $44.5\text{ }^{\circ}\text{C}$. The most severe positive temperature gradient occurred between the track slab and CA mortar.

Figure 4d shows that the vertical temperature gradient between the track slab and the CA mortar layer was positive with minimum value of $10.0\text{ }^{\circ}\text{C}\cdot\text{m}^{-1}$, which occurred at 6:00, and the maximum value of $22.5\text{ }^{\circ}\text{C}\cdot\text{m}^{-1}$ occurred at 18:30. The vertical temperature gradient between the CA mortar layer and the bottom base was negative with minimum value of $-15.0\text{ }^{\circ}\text{C}\cdot\text{m}^{-1}$, which occurred at 14:30, and the maximum value of $-25.0\text{ }^{\circ}\text{C}\cdot\text{m}^{-1}$ occurred at 9:00. The most critical positive vertical temperature gradient occurred between the track slab and the CA mortar layer, and the most critical negative vertical temperature gradient occurred between the CA mortar layer and the bottom base.

3.3. Vertical Temperature Distribution

To accurately describe the vertical temperature distribution in the CRTS-II ballastless track, the vertical temperature distributions of the EHT test and the CHT test are shown in Figure 5.

From Figure 5a, it can be seen that at the initial state of the EHT test, the temperatures in the track layers were almost equal, and the temperature curves showed a vertical nonlinear three-stage trend. The temperature–time curves of the CA mortar layer which is at a distance of 50–80 mm from the top surface of the track slab were even, indicating that the CA mortar layer showed heat insulation effects to reduce the heat conducted from the track slab top surface to the bottom base.

From Figure 5b, it can be seen that the vertical temperature distribution in the natural temperature dropping period of the EHT test was same as that in the temperature rising period, and also has a nonlinear three-stage trend. Because the natural temperature dropping rate of the CA mortar layer was slow, the thermal insulation effect on the bottom base was initiated, and when the temperature of the track slab decreased, the CA mortar reduced the heat loss from the bottom base. As the temperature of the track slab continued to decrease, the temperature of the upper part of the track slab became gradually lower than the middle part, and a negative temperature difference appeared in the track slab.

According to Figure 5c, at different moments of the CHT test, the vertical temperature distributions in the track layers were similar, and the overall vertical temperature distribution curves were in the shape of “S”. The distribution curves developed in the same direction at different moments, and the temperature was the smallest in the track layers at approximately 10:00. The highest temperature occurred in the layers between 20:00 and 0:00.

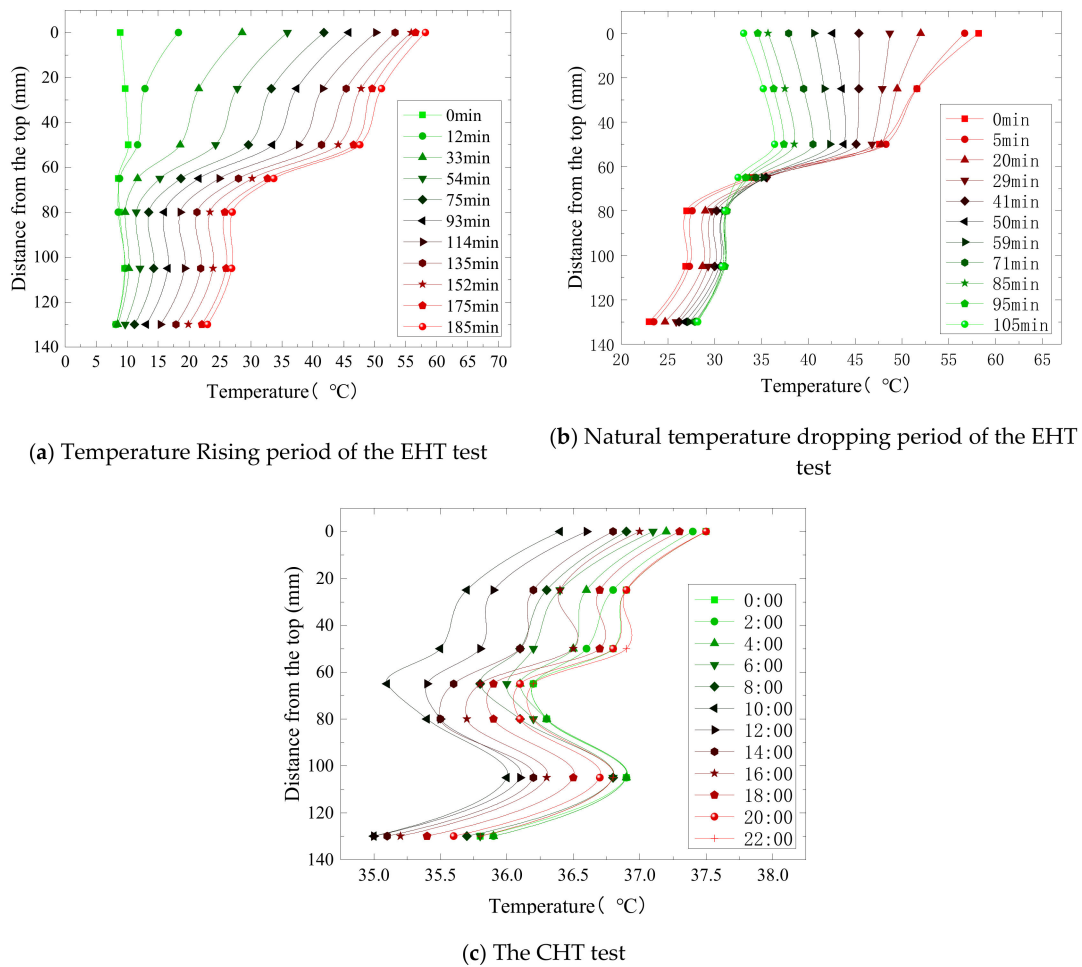


Figure 5. Vertical temperature distribution curves of the track.

To study and compare the vertical temperature distributions of the CRTS-II ballastless track on the HSR bridge under different test conditions, the vertical temperature distribution curves when the maximum temperatures occurred (the end of the temperature rising period in the EHT test and 20:00 in the CHT test) were listed, and quadratic multinomial fitting was performed by the least square method (the correlation coefficient of the fitting result was 1). Furthermore, the results were compared with the positive vertical temperature load model (Model 1) of the CRTS-II ballastless track in the Changsha area [30], as shown in Figure 6.

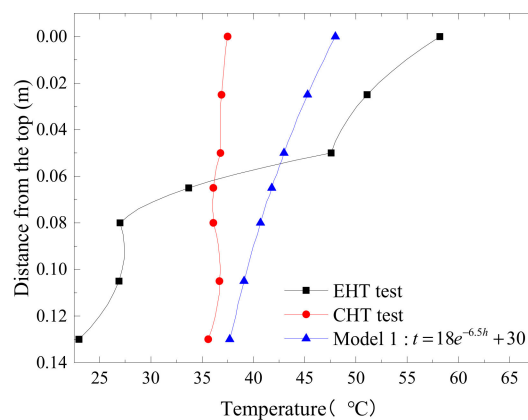


Figure 6. Comparison of the vertical temperature distribution.

The Figure 6 shows that the minimum and maximum temperatures are, respectively, 37.7 °C and 48 °C of those in the Model 1 [30]; 23 °C and 58.2 °C in the EHT test; and 35.6 °C and 37.5 °C in the CHT test. The temperature distributions obtained from the EHT test and CHT test in this paper have nonlinear, three-stage trends—which is quite different from the exponential distribution of Model 1. There are two main reasons for this difference: On one hand, the Model 1 lacked the thermodynamic parameters of the CA mortar and did not consider the influence of the CA mortar layer on the vertical temperature distribution. On the other hand, the ultimate high temperature could be simulated by the EHT test; thus, the temperature variation range in the EHT test was much larger than that of the Model 1.

The CHT test simulated the no direct sunshine high temperature conditions in summer; thus, the temperature variation range was smaller than that of the Model 1. The vertical temperature distribution curves obtained by the EHT test and CHT test were very consistent; the only difference is that the EHT test was carried out in winter with a low initial temperature, high final temperature, large temperature variation range and local heating region (the heating results obtained were local to the track on HSR bridge), while the CHT test was carried out in summer with a high initial and final temperatures, small temperature difference and temperature variation range. The most significant aspect was that the temperature of the box girder and the track changed simultaneously under the natural climate; therefore, the overall CHT test results of the track on HSR bridge were obtained.

Furthermore, the results show that the vertical temperature distribution curves of both the EHT test and the CHT test emerged over a large span in the CA mortar layer. Therefore, the temperature difference between the track slab and the bottom base was abnormal and the heat transmitting of the CA mortar was blocked. Thus, the temperature gradient effect on the different layers was abnormal and remarkable, and this could lead to the generation of interlayer separation in the track. The influence of the CA mortar layer in the design and study of the temperature effect on the track slab should then be considered carefully.

3.4. Vertical Temperature Difference Distribution

To further study the vertical temperature difference distribution in the track, the vertical temperature difference distribution of the EHT test and CHT test are shown in Figure 7.

Figure 7a shows that the vertical temperature difference of the track has nonlinear, three-stage trend and the temperature difference between the top and the bottom of the track was as high as 36.0 °C. The temperature difference curves were large in the CA mortar layer and the temperature gradient was remarkable.

Figure 7b shows that the vertical temperature difference in the natural temperature dropping period of the EHT test also has a nonlinear, three-stage trend, and changed significantly in the middle of the CA mortar layer. As the temperature decreased, the temperature difference in the middle part of the track became gradually larger than that in the upper part, and the temperature difference distribution curves tended to be consistent with the initial heating time.

Figure 7c shows that the vertical temperature difference distribution trend is similar in the track layers at different times of the CHT test and the overall vertical temperature difference distribution curves is in the shape of an “S”. The highest temperature difference between the top and bottom of the track was 1.9 °C. The variation of the temperature difference curves was large, and the temperature gradient was remarkable in the CA mortar layer.

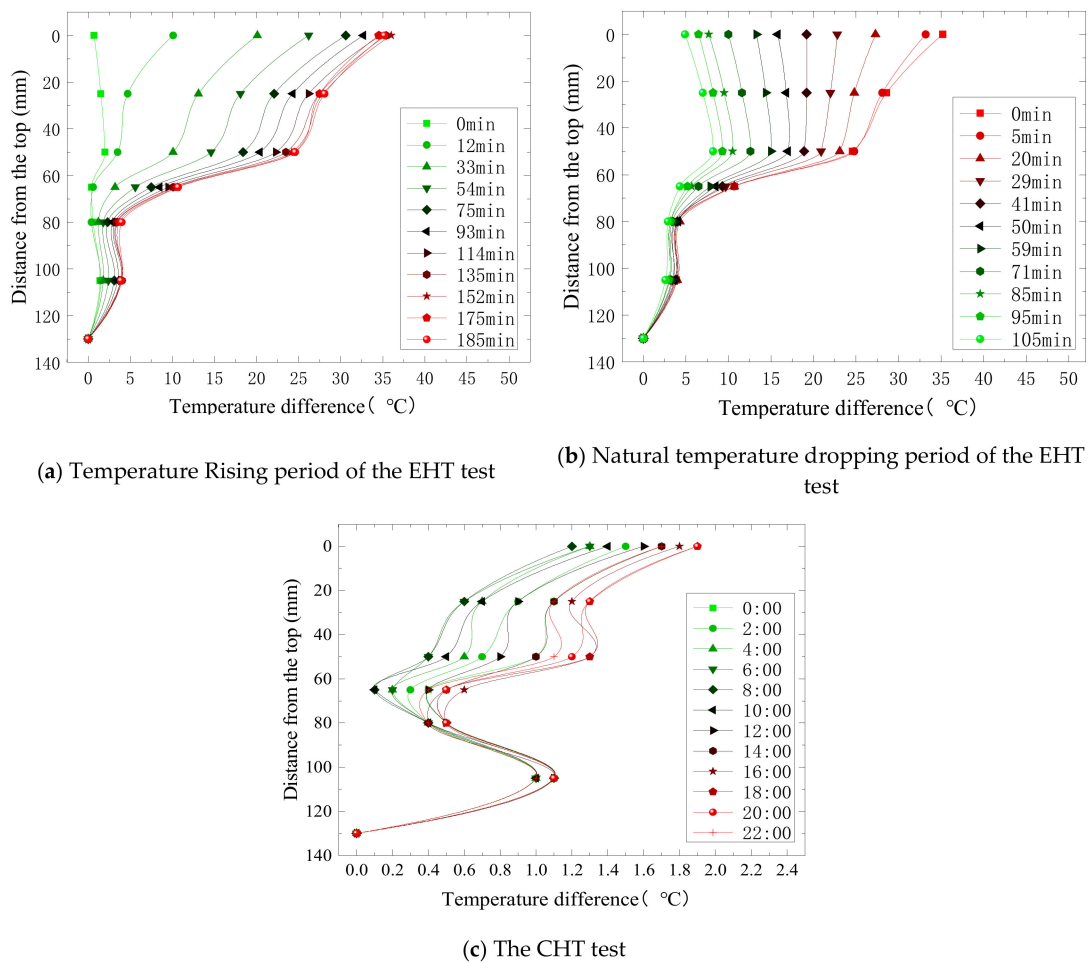


Figure 7. Vertical temperature difference distribution.

Furthermore, the vertical temperature distribution curves when the maximum temperatures occurred (the end of the temperature rising period in the EHT test and 20:00 in the CHT test) are listed, and quadratic multinomial fitting was performed by the least square method (the correlation coefficient of the fitting results was 1). The results were compared to the positive temperature difference distribution of the Model 2 [22] (CRTS-I double block ballastless track) and to the positive vertical temperature difference curves of the Model 3 [29] (CRTS-II ballastless track on sunny day), as shown in Figure 8.

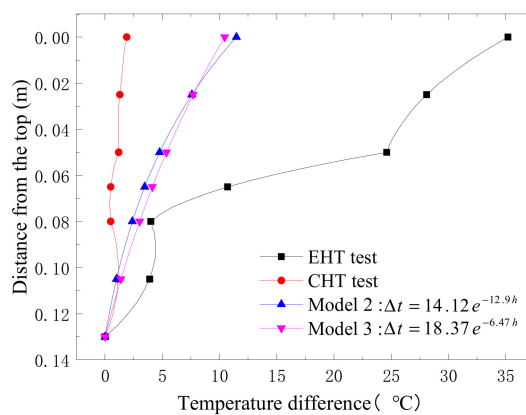


Figure 8. Comparison of the vertical temperature difference distribution.

The Figure 8 shows that the maximum temperature differences of Model 2 [22] and Model 3 [29] were 11.5 °C and 10.5 °C, respectively, while those of the EHT test and the CHT test was 35.2 °C and 1.9 °C, respectively. The temperature difference distribution curves of the Model 2 and Model 3 in Figure 8 were both exponential and similar to the tests results, indicating that under natural conditions the vertical temperature difference distribution of the CRTS-II ballastless track is similar to that of the CRTS-I double block ballastless track. The temperature difference distribution obtained from the EHT test and the CHT test have both a nonlinear, three-stage trend, which is quite different from the exponential distribution of the CRTS-II ballastless track on sunny day in the Model 3. This is because the density of vertical gauges in the test of Dai et al. [29] was smaller to that in both tests in this paper, and there were no gauges arranged in the CA mortar layer such that temperature data of the CA mortar layer were not valuable.

In addition, the study of Dai et al. [29] was conducted on an ultra-high ballastless track, and the uniformity of the arrangement of the gauges was insufficient; thus, the complete vertical temperature difference distribution in the track was not formed. Furthermore, the EHT test was designed to simulate the ultimate high temperature load that the CRTS-II ballastless track could achieve, and the CHT test was designed to simulate the thermal behavior of the CRTS-II ballastless track under no direct sunshine conditions in summer, while the Model 3 provided the thermal behavior of the CRTS-II ballastless track under direct solar irradiation on sunny day. Therefore, the vertical maximum temperature difference of the CRTS-II ballastless track in the EHT test was much larger than that in Model 3, and the vertical maximum temperature difference of the CRTS-II ballastless track in the CHT test was smaller than that in Model 3.

4. Transverse Temperature Distribution and Laws

4.1. Transverse Temperature Distribution

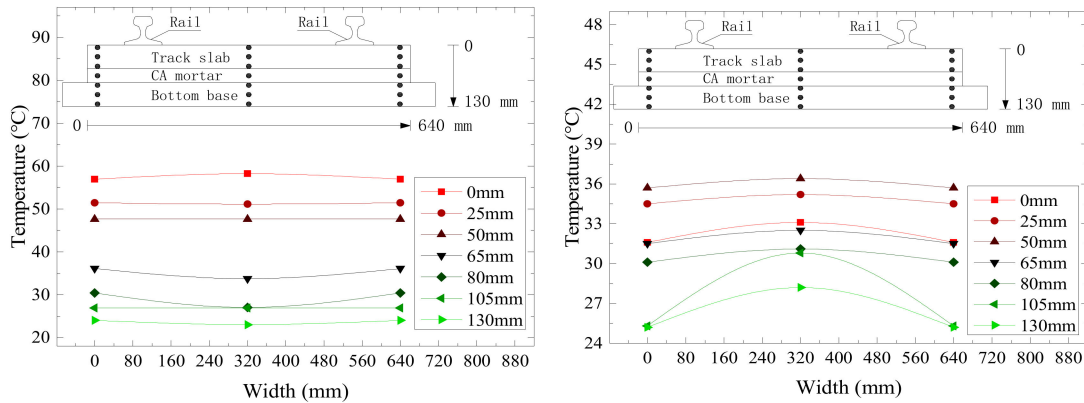
To study the transverse temperature distribution in the track, the moments at which the maximum temperatures occurred (the end of the temperature rising period in the EHT test and 20:00 in the CHT test) and those at which the minimum temperature occurred (the end of the natural temperature dropping period in the EHT test) are plotted, as shown in Figure 9. The transverse temperatures at the edges of the track were the same due to the uniform heating.

Figure 9a shows that during the EHT test, the top surface temperature of the track slab is slightly higher at the cross-section middle than the edges in the temperature rising period, while the temperature of the bottom surface and that of the center of the track slab layer were basically same at the cross-section middle and the edges. The bottom surface temperature and the center temperature of the CA mortar layer were smaller at the cross-section middle than the edges. The transverse temperature distribution was of concave parabolic trend and the maximum negative temperature difference was −3.4 °C (the temperature difference is considered positive when the temperature at the cross-section middle is larger than the edges; otherwise it is considered negative). The temperature of the bottom surface and that of the center of the bottom base layer were basically identical at the cross-section middle and the edges.

Figure 9b shows that during the temperature dropping period of the EHT test, the temperature in the track layers was higher at the cross-section middle than that at its edges and the transverse temperature distribution was of convex parabolic trend, resulting in positive transverse temperature difference. The maximum positive transverse temperature differences of the track slab, CA mortar layer and bottom base were 1.5 °C, 1.1 °C and 5.5 °C, respectively; thus, the transverse temperature gradient of the bottom base was the highest.

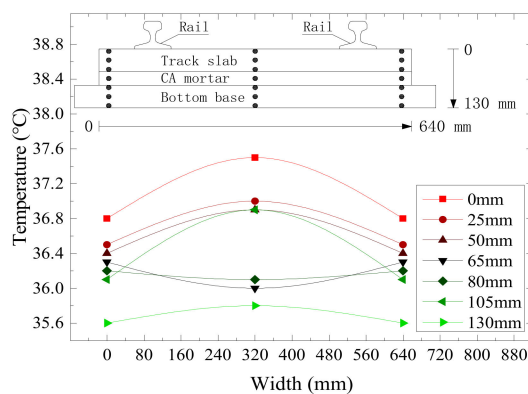
Figure 9c shows that at moment that the maximum temperature occurred in the CHT test, the temperature of the track slab was higher at the cross-section middle than the edges. The transverse temperature distribution was of convex parabolic trend with a maximum positive temperature difference of 0.8 °C. The bottom surface temperature and center temperature of the CA mortar layer

were smaller at the cross-section middle than the edges, with concave parabolic distribution trends and a maximum negative temperature difference of $-0.5\text{ }^{\circ}\text{C}$. The bottom surface temperature and center temperature of the bottom base layer were higher at the cross-section than the edges, with convex parabola distribution trends and a maximum positive temperature difference of $0.7\text{ }^{\circ}\text{C}$.



(a) Temperature Rising period of the EHT test

(b) Natural temperature dropping period of the EHT test



(c) The CHT test

Figure 9. Transverse temperature distribution.

Combined with the analysis of the vertical temperature distribution, it could be concluded that the transverse temperature distribution in the track was of quadratic parabolic trend. The CA mortar showed heat insulation and heat preservation performance. The vertical temperature conduction in the CA mortar layer was blocked, and it was difficult to transmit heat from the top surface to the middle and bottom surface of the CA mortar. Therefore, when the air temperature increased, the external temperature of the CA mortar layer was higher than the internal temperature, and the transverse temperature distribution had a concave parabolic trend. When the air temperature decreased, it was difficult to transmit outside of the CA mortar, which was fully endothermic and heated such that the CA mortar layer showed a continuous heating and heat preservation effect on the track slab and the bottom base. In addition, the temperature in track layers was higher at the cross-section middle than the edges, and the transverse temperature distribution had a quadratic parabolic trend. In conclusion, the CA mortar layer and box girder are the most important factors influencing the transverse temperature distribution in the track on HSR bridge.

4.2. Transverse Temperature Difference and Temperature Gradient

To describe the change law of the transverse temperature difference of the track during the whole test process, the transverse temperature difference and temperature gradient in the track layers were studied and analyzed, as shown in Figure 10.

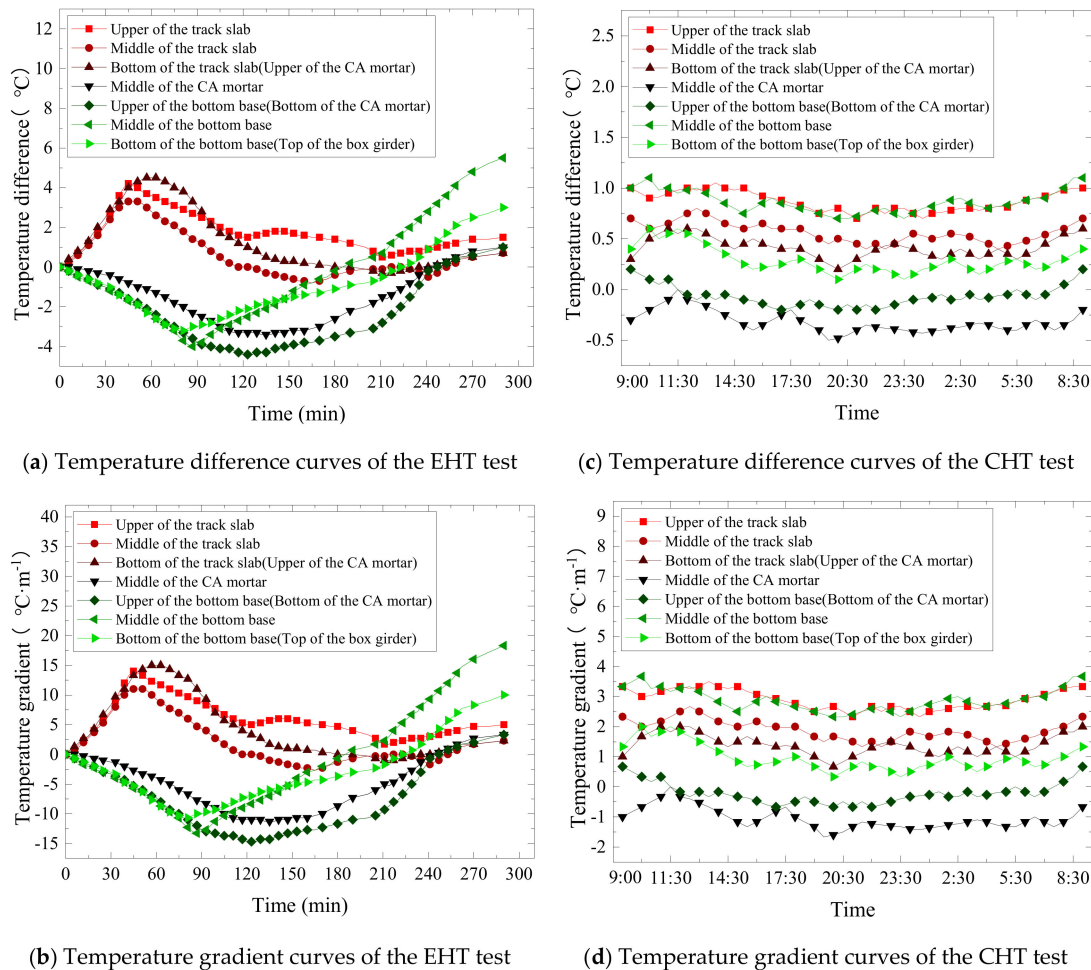


Figure 10. Transverse temperature difference and temperature gradient curves of the track.

Figure 10a shows that the transverse temperature difference of the track slab in the EHT test was positive, with a maximum temperature difference of 4.5 °C occurring at the bottom surface of the layer. The temperature difference first increased and then decreased to zero. The CA mortar layer was mainly affected by the negative transverse temperature difference, which first increased and then decreased, and finally appeared as a small positive temperature difference with a maximum value of −4.4 °C at the bottom surface of the layer. In the temperature rising period of the EHT test, the bottom base was mainly affected by a negative transverse temperature difference, which also first increased and then decreased with a maximum value of −4.0 °C at the center of the layer, while in the natural temperature dropping period of the EHT test, the bottom base was mainly affected by a positive transverse temperature difference with a maximum value of 5.5 °C occurring at the center of the layer.

Figure 10b shows that the transverse temperature gradient of the layers in the EHT test was similar to the transverse temperature difference. The track slab was mainly affected by a positive transverse temperature gradient, which first increased and then decreased to zero with a maximum value of 15.0 °C·m⁻¹ occurring at the bottom surface of the layer. The CA mortar layer was mainly affected by a negative transverse temperature gradient, which first increased and then decreased to zero with a maximum value of −14.7 °C·m⁻¹ occurring at the bottom surface of the layer. In the temperature rising

period of the EHT test, the bottom base was mainly affected by a negative transverse temperature gradient, which first increased and then decreased with a maximum value of $-13.3\text{ }^{\circ}\text{C}\cdot\text{m}^{-1}$ occurring at the center of the layer; however, in the temperature dropping period of the same test, the bottom base was mainly affected by a positive transverse temperature gradient, which tended to increase gradually and reached a maximum temperature gradient of $18.3\text{ }^{\circ}\text{C}\cdot\text{m}^{-1}$ at the center of the layer.

Figure 10c shows that the transverse temperature difference in the CHT test is periodic. The transverse temperature difference in the track slab is positive and decreases gradually from the top surface to the bottom surface of the track slab, with a maximum value of $1.1\text{ }^{\circ}\text{C}$ occurring on the top surface of the track slab at 13:00. The bottom surface and the center of the CA mortar layer were mainly affected by a negative transverse temperature difference, which decreased gradually from the top surface to the bottom surface of the layer, with a maximum value of $-0.5\text{ }^{\circ}\text{C}$ occurring at the center of the layer at 19:30. The temperature difference also decreased gradually from the top surface to the bottom surface of the bottom base, with a maximum value of $1.1\text{ }^{\circ}\text{C}$ occurring at the center of the layer at 9:00.

Figure 10d shows that in the CHT test, the transverse temperature gradient in the track layers was similar to the transverse temperature difference. The track slab was mainly affected by a positive transverse temperature gradient with a maximum value of $3.5\text{ }^{\circ}\text{C}\cdot\text{m}^{-1}$ occurring on the top surface of the layer at 13:00. The bottom surface and center of the CA mortar layer were mainly affected by a negative transverse temperature gradient, which decreased gradually from the center to the bottom surface of the CA mortar with a maximum value of $-1.7\text{ }^{\circ}\text{C}\cdot\text{m}^{-1}$ occurring at 19:30. The bottom surface and the center of the bottom base were mainly affected by a positive transverse temperature gradient, which decreased gradually from the center to the bottom surface of the bottom base, with a maximum value of $3.7\text{ }^{\circ}\text{C}\cdot\text{m}^{-1}$ occurring layer at 9:00.

The analysis results of the transverse temperature difference and the temperature gradient further show that under no direct sunshine high temperature conditions, the CA mortar layer was mainly affected by a negative temperature gradient because of the effect of its own thermal insulation and heat preservation characteristics, while the track slab and the bottom base were mainly affected by a positive transverse temperature gradient. The positive and the negative transverse temperature gradient were very significant at the interlayer interfaces, and the influence of the CA mortar layer on the transverse temperature gradient of the track was very significant.

5. Three-Dimensional Temperature Distribution

To describe the three-dimensional comprehensive distribution of the transverse and vertical temperature of the CRTS-II ballastless track on the HSR bridge, the track was sorted into a three-dimensional distribution surface along the transverse width and the vertical depth (distance from top surface of the track slab). The three-dimensional distributions are shown in Figure 11—when the maximum and minimum temperatures occurred in the EHT test and the CHT test.

Figure 11a shows that the vertical temperature distribution in the track during the temperature rising period in the EHT test was a nonlinear three-stage surface. The temperature difference in the bottom of the track was large. The vertical temperature changed greatly, and the order of magnitude of the transverse temperature difference was much smaller than that of the vertical temperature difference.

Figure 11b shows that the three-dimensional temperature distribution in the track during the temperature dropping period in the EHT test was also a nonlinear, three-stage surface. However, due to the convex parabolic trend of the transverse temperature distribution in the temperature dropping period, the three-dimensional temperature distribution at the bottom part of the track presented a saddle-shaped surface; meanwhile, the upper part of the track slab presented a turning point showing a duck tongue surface. This indicates that the transverse temperature variation was in the same order of magnitude as the vertical temperature in the temperature dropping period of the EHT test, and the transverse temperature has a great influence on the overall temperature distribution of the track in this stage.

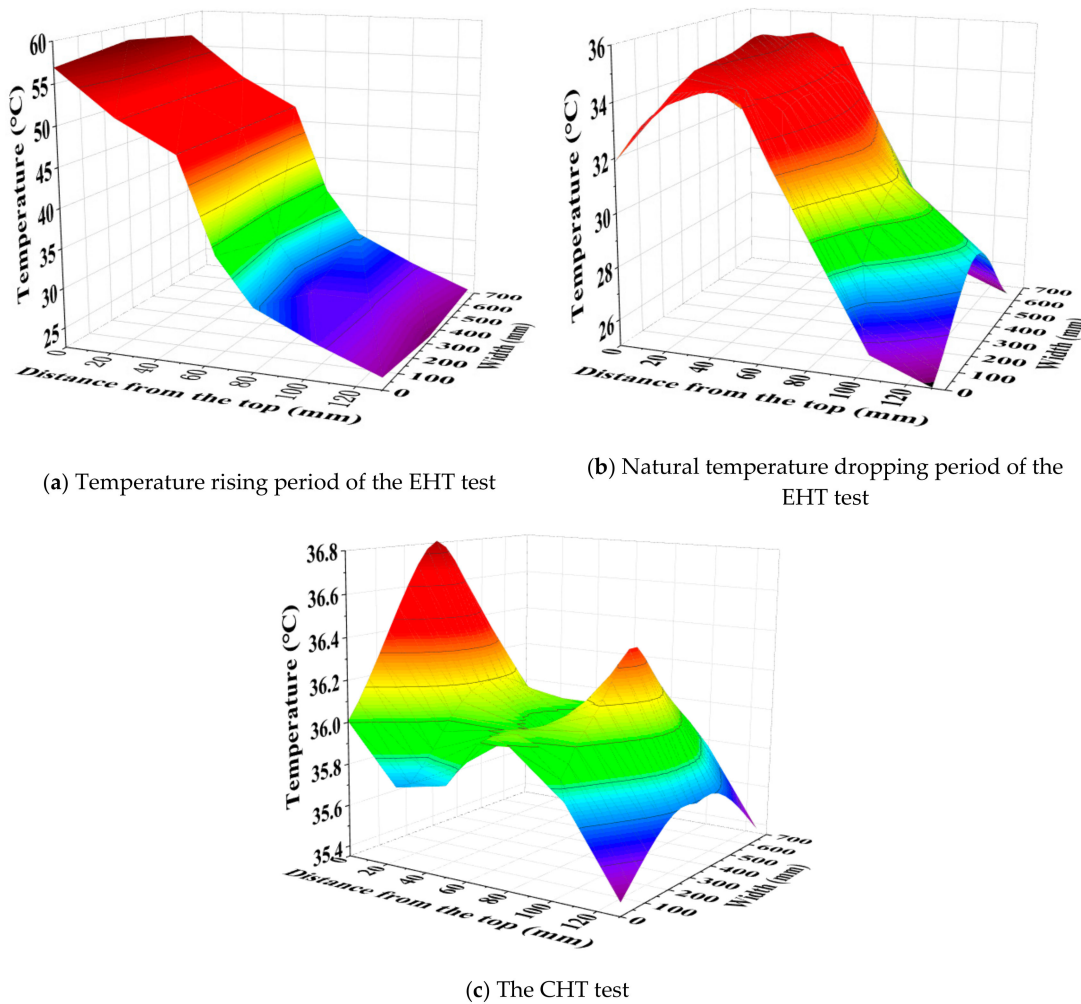


Figure 11. 3D temperature distribution in the track.

Figure 11c shows that in the natural temperature period, the overall three-dimensional temperature distribution of the track under no direct sunshine high temperature conditions was a double-hump saddle surface. Because the transverse and vertical temperature difference are of the same order of magnitude, the transverse temperature distribution has a significant impact on the overall temperature distribution of CRTS-II ballastless track; thus, the three stages of the vertical temperature distribution were covered up. As the CA mortar showed heat insulation effect. Therefore, the CA mortar layer was the main factor influencing the three-dimensional temperature distribution in the track. The effect of the CA mortar layer on the thermal performance of the track should be considered carefully in the design of the track slabs.

6. Discussions

To assess the developed temperatures in the real track, the cross-section factor α (exposed to temperature area/volume of the track) was introduced in this paper, and this provides a reference for the temperature distribution of the real track. The calculation process is shown in Equation (1).

$$\alpha = A/V = L/S \tag{1}$$

where α denotes the section factor of the track, A denotes the heating area of the track exposed to atmosphere, V denotes the heating volume of the track, L denotes the cross-section length of the track exposed to the atmosphere, and S denotes the cross-section area of the track. According to the results of

the above equation, the scaled specimen and the prototype were compared and analyzed, as shown in Table 1.

Table 1. The section factor.

Projects	L (mm)	S (mm ²)	α (mm ⁻¹)	α_s/α_p
Scaled specimen	900	88,200	0.0102	3.52
Prototype	3420	1,180,800	0.0029	

From the Table 1, it can be seen that the ratio of the section factor between the scaled specimen and the prototype structure of the track is 3.52, which indicates that the temperature gradient change of the scaled specimen is greater than that of the prototype structure. It can be roughly considered that under the same external heat source conditions, the temperature difference and temperature gradient change of the scaled specimen is about 3.52 times that of the prototype. The results can be used as reference for the temperature distribution in a real track.

It should be pointed out that because the scaled specimen in this paper is smaller than the prototype structure (only the thickness of CA mortar layer in the scaled specimen is the same as the prototype), the temperature transfer rate between the layers in the scaled specimen might be faster than that in the prototype structure. However, because of the geometric similarities between the scaled specimen and the prototype structure, the temperature distribution results obtained in this paper are also similar to the actual temperature distribution of the prototype structure; thus, the laws obtained in this study could be reflected in the prototype structure.

7. Conclusions

By means of the extreme high temperature (EHT) test in winter and conventional temperature (CHT) test in summer, the temperature distribution in the CRTS-II ballastless track on HSR bridge was studied. The results show the following conclusions:

- (1) According to the EHT test and the CHT test, there is an obvious difference in the temperature conduction in the different layers of the track, and the greater the depth from the top surface of the track slab, the more obvious the temperature conduction lag.
- (2) In summer, the internal temperature gradient in the different of the track layers is positive and changes periodically (every 24 h). The bottom base is the less affected by the vertical temperature gradient in the track. The CA mortar layer shows heat insulation and preservation effects in the different test conditions, and is the layer the most affected by the vertical temperature gradient in the track.
- (3) The vertical temperature distribution in the track has a nonlinear, three-stage trend and the heat conduction in the CA mortar layer is blocked; therefore, the temperature gradient effect in the track is very significant.
- (4) The transverse temperature distribution in the different layers of the CRTS-II ballastless track has a quadratic parabolic trend, and the CA mortar layer is the most significant factor affecting the transverse temperature distribution in the track.
- (5) The CA mortar layer exhibits a heat insulation effect to reduce the heat loss. At the same time, the concrete box girder also exhibits continuous temperature preservation performance in the bottom base when the air temperature decreases.
- (6) In the EHT test, when the air temperature increases rapidly, the three-dimensional temperature distribution in the track has a nonlinear three-stage surface trend, and when the air temperature decreases rapidly, the three-dimensional temperature distribution in the bottom part of the track has a saddle-shaped surface trend. The distribution in the upper part has a duck-tongue surface trend. Under the no direct sunshine high temperature conditions of the CHT

test, the three-dimensional temperature distribution in the track has a double hump saddle surface trend.

Author Contributions: Conceptualization, L.Z., L.-Y.Z., G.-C.Z., T.-Y.W., A.D.M., Y.-Y.Z. and L.-Q.J.; data curation, L.Z., G.-C.Z., Y.-Y.Z. and A.D.M.; formal analysis, L.Z., L.-Y.Z., T.-Y.W., G.-C.Z. and L.-Q.J.; funding acquisition, L.-Y.Z., L.Z., G.-C.Z., Y.-Y.Z., T.-Y.W. and L.-Q.J.; investigation, L.-Y.Z., L.Z., T.-Y.W., Y.-Y.Z., G.-C.Z. and L.-Q.J.; methodology, L.-Y.Z., L.Z., T.-Y.W., G.-C.Z., A.D.M. and L.-Q.J.; project administration, L.-Y.Z. and L.Z.; resources, A.D.M. and L.Z.; software, L.-Y.Z. and A.D.M.; supervision, L.Z., T.-Y.W. and A.D.M.; Validation, L.-Q.J., L.Z., G.-C.Z. and Y.-Y.Z.; visualization, L.-Y.Z., G.-C.Z., A.D.M., L.Z. and L.-Q.J.; writing—original draft, L.Z., L.-Y.Z. and A.D.M.; writing—review and editing, L.Z., L.-Y.Z. and L.-Q.J. All authors have read and agreed to the published version of the manuscript.

Funding: This research was funded by the National Natural Science Foundation of China, grant numbers 51578546 and 51878674; and the National Science Joint High-Speed Railway Foundation of China, grant numbers U1434204 and U1934217.

Acknowledgments: Special thanks are extended to the reviewers for their valuable suggestions. The authors would like to thank the National Engineering Laboratory of High-Speed Railway Construction Technology of China, the staff of the laboratory for their help in the smooth development of the experiment and the reviewers for their hard work.

Conflicts of Interest: The authors declare no conflicts of interest.

References

1. Zhou, L.Y.; Yang, L.Q.; Shan, Z.; Peng, X.S.; Akim, D.M. Investigation of the fatigue behaviour of a ballastless slab track-bridge structure system under train load. *Appl. Sci.* **2019**, *9*, 3625. [[CrossRef](#)]
2. Ramos, Ó.R.; Schanack, F.; Ortega Carreras, G.; de Vena Retuerto, J. Bridge length limits due to track-structure interaction in continuous girder prestressed concrete bridges. *Eng. Struct.* **2019**, *196*, 109310. [[CrossRef](#)]
3. Gautier, P.E. Slab track: Review of existing systems and optimization potentials including very high speed. *Construction. Build. Mater.* **2015**, *92*, 9–15. [[CrossRef](#)]
4. Liu, X.Y.; Zhao, P.R.; Dai, F. Advances in design theories of high-speed railway ballastless tracks. *J. Modern Transp.* **2011**, *19*, 154–162. [[CrossRef](#)]
5. Jiang, L.Q.; Ye, J.H.; Zheng, H. Collapse mechanism analysis of the FIU pedestrian bridge based on the improved structural vulnerability theory (ISVT). *Eng. Fail. Anal.* **2019**, *104*, 1064–1075. [[CrossRef](#)]
6. Liu, J.; Liu, Y.J.; Zhang, G.J. Experimental analysis of temperature gradient patterns of concrete-filled steel tubular members. *J. Bridge Eng.* **2019**, *24*, 04019109. [[CrossRef](#)]
7. Kim, S.H.; Cho, K.I.; Won, J.H.; Kim, J.H. A study on thermal behaviour of curved steel box girder bridges considering solar radiation. *Arch. Civ. Mech. Eng.* **2009**, *9*, 59–76. [[CrossRef](#)]
8. Xia, Q.; Zhang, J.; Tian, Y.D.; Zhang, Y.F. Experimental study of thermal effects on a long-span suspension bridge. *J. Bridge Eng.* **2017**, *22*, 04017034. [[CrossRef](#)]
9. Mirambell, E.; Aguado, A. Temperature and stress distributions in concrete box girder bridges. *J. Struct. Eng.* **1990**, *116*, 2388–2409. [[CrossRef](#)]
10. Hagedorn, R.; Martí-Vargas, J.R.; Dang, C.N.; Hale, W.M.; Floyd, R.W. Temperature gradients in bridge concrete i-girders under heat wave. *J. Bridge Eng.* **2019**, *24*, 04019077. [[CrossRef](#)]
11. Abid, S.R.; Taysi, N.; Özakça, M. Experimental analysis of temperature gradients in concrete box-girder. *Constr. Build. Mater.* **2016**, *106*, 523–532. [[CrossRef](#)]
12. Lawson, L.; Ryan, K.L.; Buckle, I.G. Bridge Temperature Profiles Revisited: Thermal analyses based on recent meteorological data from Nevada. *J. Bridge Eng.* **2020**, *25*, 04019124. [[CrossRef](#)]
13. Elbadry, M.M.; Ghali, A. Temperature variations in concrete bridges. *J. Struct. Eng.* **1983**, *109*, 2355–2374. [[CrossRef](#)]
14. Zhu, J.S.; Meng, Q.L. Effective and fine analysis for temperature effect of bridges in natural environments. *J. Bridge Eng.* **2017**, *22*, 04017017. [[CrossRef](#)]
15. Song, X.; Melhem, H.; Li, J.; Xu, Q.; Cheng, L. Effects of solar temperature gradient on long-span concrete box girder during cantilever construction. *J. Bridge Eng.* **2016**, *21*, 04015061. [[CrossRef](#)]
16. Zhong, Y.L.; Gao, L.; Wang, P.; Wang, S.J. Mechanism of interfacial shear failure between CRTS-II slab and CA mortar under temperature loading. *J. Eng. Mech.* **2018**, *35*, 230–238. (In Chinese) [[CrossRef](#)]

17. Yang, R.S.; Li, J.L.; Kang, W.X.; Liu, X.Y.; Cao, S.H. Temperature characteristics analysis of the ballastless track under continuous hot weather. *J. Transp. Eng. Part A Syst.* **2017**, *143*, 04017048. [[CrossRef](#)]
18. Yu, Z.W.; Xie, Y.; Tian, X.Q. Research on mechanical performance of CRTS-III plate-type ballastless track structure under temperature load based on probability statistics. *Adv. Civ. Eng.* **2019**, *8*, 1–16. [[CrossRef](#)]
19. Zeng, Z.P.; Huang, Z.B.; Yin, H.T.; Meng, X.B.; Wang, W.D.; Wang, J.D. Influence of track line environment on the temperature field of a double-block ballastless track slab. *Adv. Mech. Eng.* **2018**, *10*. [[CrossRef](#)]
20. Liu, X.Y.; Li, J.L.; Kang, W.X.; Liu, X.K.; Yang, R.S. Simplified calculation of temperature in concrete slab of ballastless track and influence of extreme weather. *J. Southwest Jiaotong Univ.* **2017**, *52*, 1037–1045. (In Chinese) [[CrossRef](#)]
21. Li, J.; Zhao, P.R.; Wan, Z.B.; Ren, B. Experimental research and numerical analysis of temperature field on bi-block ballastless track. *Chin. Sci. Technol. Sci.* **2014**, *44*, 729–735. [[CrossRef](#)]
22. Yang, R.S.; Wan, Z.B.; Liu, X.Y.; Zhang, C.W.; Zhao, R.P. Temperature field test of CRTS-I twin-block ballastless track in winter. *J. Southwest Jiaotong Univ.* **2015**, *50*, 454–460. (In Chinese) [[CrossRef](#)]
23. Shan, Y.C.; Zheng, S.G.; Zhang, X.F.; Luo, W.; Mao, J.D.; Kong, D.Y. Fatigue performance of the CA mortar used in CRTS-I ballastless slab track under simulated servicing condition. *Materials* **2018**, *11*, 2259. [[CrossRef](#)] [[PubMed](#)]
24. Ren, J.J.; Li, X.; Yang, R.S.; Wang, P.; Xie, P. Criteria for repairing damages of CA mortar for prefabricated framework-type slab track. *Constr. Build. Mater.* **2016**, *110*, 300–311. [[CrossRef](#)]
25. Rutherford, T.; Wang, Z.J.; Shu, X.; Huang, B.S.; Clarke, D. Laboratory investigation into mechanical properties of cement emulsified asphalt mortar. *Constr. Build. Mater.* **2014**, *65*, 76–83. [[CrossRef](#)]
26. Zumin, O.; Fujian, L. Analysis and prediction of the temperature field based on insitu measured temperature for CRTS-II ballastless track. *Energy Procedia* **2014**, *61*, 1290–1293. [[CrossRef](#)]
27. Cai, X.P.; Lou, B.C.; Zhong, Y.L.; Zhang, Y.R.; Hou, B.W. Arching mechanism of the slab joints in CRTS-II slab track under high temperature conditions. *Eng. Fail. Anal.* **2019**, *98*, 95–108. [[CrossRef](#)]
28. Zhao, L.; Sun, L.; Fan, T.J. Temperature field analysis of CRTS-II ballastless track slab structure on soil subgrade. *Appl. Mech. Mater.* **2014**, *587–589*, 1255–1261. [[CrossRef](#)]
29. Dai, G.L.; Su, H.T.; Liu, W.S.; Yan, B. Temperature distribution of longitudinally connected ballastless track on bridge in summer. *J. Cent. South Univ. Sci. Technol.* **2017**, *48*, 1073–1080. (In Chinese) [[CrossRef](#)]
30. Yan, B.; Liu, S.; Dai, G.L.; Pu, H. Vertical nonlinear temperature distribution and temperature mode of ballastless track in typical areas of China. *J. Railw. Soc.* **2016**, *38*, 81–86. (In Chinese) [[CrossRef](#)]
31. Zhu, J.S.; Guo, X.D.; Meng, Q.L. Analysis of fine temperature field for bridge-track system of high-speed railway. *China Railw. Sci.* **2019**, *40*, 36–45. (In Chinese) [[CrossRef](#)]
32. Lou, P.; Zhu, J.P.; Dai, G.L.; Yan, B. Experimental study on bridge-track system temperature actions for Chinese high-speed railway. *Arch. Civ. Mech. Eng.* **2018**, *18*, 451–464. [[CrossRef](#)]
33. China Railway Design Code. *Code for Design on Railway Bridges and Culvert*; TB 10002-2017; National Railway Administration of the PRC: Beijing, China. (In Chinese)

